ACS APPLIED MATERIALS & INTERFACES

www.acsami.org

Research Article

Efficient All-Dielectric Diatomic Metasurface for Linear Polarization Generation and 1-Bit Phase Control

Song Gao, Changyi Zhou, Wenjing Yue,* Yang Li,* Chunwei Zhang, Hao Kan, Chao Li, Sang-Shin Lee, and Duk-Yong Choi

Cite This: *ACS Appl. Mater. Interfaces* 2021, 13, 14497−14506

Read Online

ACCESS | Metrics & More | Article Recommendations | Supporting Information

ABSTRACT: Optical metasurface has exhibited unprecedented capabilities in the regulation of light properties at a subwavelength scale. In particular, a multifunctional polarization metasurface making use of light polarization to integrate distinct functionalities on a single platform can be greatly helpful in the miniaturization of photonic systems and has become a hot research topic in recent years. Here, we propose and demonstrate an efficient all-dielectric diatomic metasurface, the unit cell of which is composed of a pair of a-Si:H-based nanodisks and nanopillars that play the roles as polarization-maintaining and polarization-converting meta-atoms, respectively. Through rigorous theoretical analyses and numerical simulations, we show that a properly designed diatomic metasurface can work as a nanoscale linear polarizer for generating linearly polarized light with a controllable polarization angle and superior performances including a maximum transmission efficiency of 96.2% and an extinction ratio of 32.8 dB at an operation wavelength of 690 nm. Three metasurface samples are fabricated and experimentally characterized to verify our claims and their potential applications. Furthermore, unlike previously reported dielectric diatomic metasurfaces which merely manipulate the polarization state, the proposed diatomic metasurface can be easily modified to empower 1-bit phase modulation without altering the polarization angle and sacrificing the transmission efficiency. This salient feature further leads to the demonstration of a metasurface beam splitter that can be equivalently seen as the integration of a nonpolarizing beam splitter and a linear polarizer, which has never been reported before. We envision that various metadevices equipping with distinct wavefront shaping functionalities can be realized by further optimizing the diatomic metasurface to achieve an entire 2π phase control.

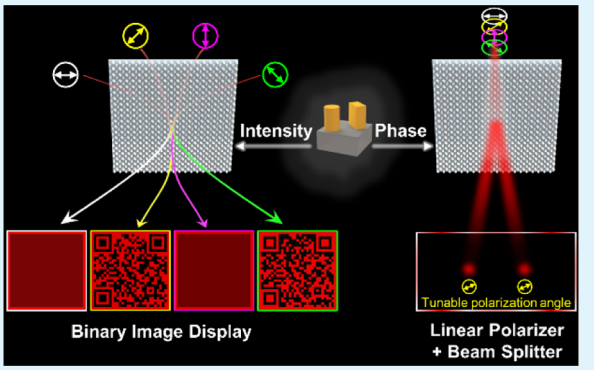

KEYWORDS: *diatomic metasurface, dielectric metasurface polarizer, metasurface beam splitter, polarization generation, 1-bit phase control*

INTRODUCTION

The planar counterpart of the three-dimensional optical metamaterial, dubbed as optical metasurface, has been extensively explored in recent years. It is usually an array consisting of periodically or quasi-periodically arranged nanostructures (also referred to as meta-atoms) that can be elaborately designed to manipulate the light properties over a subwavelength scale. The original and most fundamental core idea of metasurface lies in the introduction of an abrupt phase change or phase discontinuity across/along an interface, which has led to the generalization of the classical Snell's law and brought about the unprecedented anomalous light deflection phenomenon.[1] Over the past decade, vast research endeavors have been focused on demonstrating metadevices that can realize various wavefront shaping functionalities such as metalens,[2] metahologram,[3] and vortex beam generator.[4] Besides, the flexible design strategy has also inspired the generation of a variety of intriguing metadevices that can fulfill multiple distinct functionalities on a single platform.[5,6]

Apart from the phase property, polarization is another elemental light characteristic that plays crucial roles in affecting the strength of light−matter interaction, and its arbitrary generation and manipulation is thus of great significance considering the potential applications in scientific research fields encompassing polarimetry,[7] imaging, and display,[8] to name a few. Unfortunately, due to the use of natural materials, conventional optical polarization components such as polarizers, wave-plates, and polarizing/nonpolarizing beam splitters

Received: January 15, 2021
Accepted: March 9, 2021
Published: March 22, 2021

https://doi.org/10.1021/acsami.1c00967
ACS Appl. Mater. Interfaces 2021, 13, 14497−14506

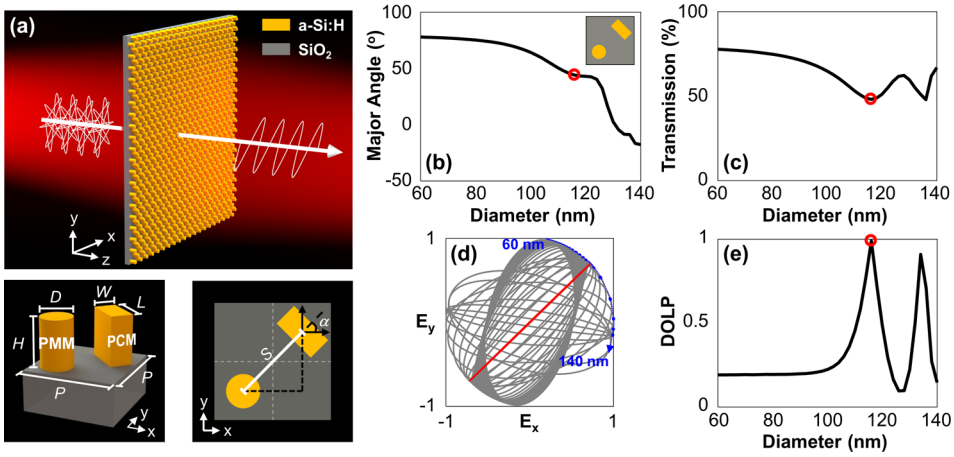

Figure 1. (a) Schematic of the proposed all-dielectric diatomic metasurface for linear polarization generation, and the perspective and top views of the metasurface UC, which is composed of the a-Si:H-based PMM and PCM. The numerical simulation results of the (b) major polarization angle, (c) transmission efficiency, (d) polarization ellipse map, and (e) DOLP of transmitted light as a function of the PMM diameter.

typically exhibit bulky volumes, which do not meet the current trend of device miniaturization and hence hinder the development of an ultracompact nanophotonic system. Metasurface also serves as a promising candidate to substitute conventional polarization components, taking account of its drastically reduced device thickness.[9−19] For example, subwavelength-thick rectangular silicon nanopillars can functionally operate as truncated waveguides allowing certain modes with polarization-dependent effective indices to propagate.[14,15] By meticulously designing its lateral dimension and orientation, a π phase difference between two orthogonal polarizations can be obtained, and consequently, a metasurface half-wave plate (HWP) that holds a linear polarization rotation/conversion function can be realized. A set of such polarization-converting meta-atoms (PCMs) imparting distinct phase delays can be used to realize the integration of wave plate and other optical components such as lens, beam splitter, and parabolic reflector. The unprecedented polarizing device that can simultaneously empower distinct polarization modulation functionalities including linear and circular dichroism on a single platform has also become feasible, further revealing its fascinating ability in polarization control.[20,21]

Recently, PCMs with spatially varying orientation angles have also been popularly used in high-resolution information encryption or anticounterfeiting applications, mostly presented as a grayscale image concealed in the polarization profile of a light beam.[22−25] Upon light illumination, the hidden image will naturally be invisible under direct observation due to a uniform intensity distribution, yet it can be revealed through an analyzer. Direct observation of high-resolution metaimages without relying on an external analyzer has also been reported by adopting metasurface-based two-dimensional nanoscale linear polarizers.[26−31] For instance, incident light with polarization parallel to the short axis of an elaborately designed rectangular silver nanorod can be transmitted, while its orthogonal counterpart will be reflected.[29] Similar polarization filtering results over broadband in the near-infrared region can be attained by adopting vertically stacked bilayer aluminum nanorods.[31] Such metasurface-based linear polarizer can empower pure light intensity manipulation at a subwavelength scale in two-dimensional directions, outperforming the conventional wire grid polarizer or thin-film linear polarizer and can find promising applications such as in generating a quick response (QR) code, a type of two-dimensional matrix barcode, presented as distinct black squares "disorderly" arranged in a square grid on the white background via meticulous design, that can store information of an item to which it is linked and can be read by scanning it using an imaging device such as the camera of a smartphone. It is recently demonstrated that an additional Pancharatnam−Berry phase can be induced by properly rotating the metasurface linear polarizer meta-atoms, which can in turn add an extra wavefront shaping functionality.[32] While the simultaneous and independent manipulation of light amplitude and phase has become feasible, yet it is known that such geometric phase-enabled wavefront control is only valid for circularly polarized light.

Incorporating multiple meta-atoms in a single unit cell (UC) is expected to provide more freedom in the metasurface design. Recently, diatomic metasurfaces consisting of two identical metallic nanorods or dissimilar dielectric nanopillars in a single UC have been proposed.[33−37] By tailoring the dimension of both nanopillars, or the spatial displacements and orientations of the nanorods, the metasurfaces are deemed to enable dispersion control, pure polarization control, or polarization-dependent vectorial holography. In this paper, we present a general method for implementing a nanoscale linear polarizer based on an all-dielectric diatomic metasurface whose UC is composed of a polarization-maintaining meta-atom (PMM) and a HWP-like PCM. Theoretical analyses and numerical simulations are systematically carried out and show that the PMM and PCM with proper dimension and orientation angle can cooperate and effectively work as a linear polarizer with high transmission efficiency and a controllable polarization angle. Several metasurface samples are fabricated and characterized to verify our claims and its potential application in generating a QR code. Without altering its polarization angle, we further demonstrate that the proposed metasurface can efficiently impart a relative π phase delay to transmitted light by simply changing the PMM diameter and PCM orientation angle. This feature further enables the realization of a metasurface beam splitter which is equivalent to the integration of a linear polarizer and nonpolarizing beam splitter. We anticipate that more diatomic metasurface UCs

https://doi.org/10.1021/acsami.1c00967
ACS Appl. Mater. Interfaces 2021, 13, 14497−14506

can be designed to cover the 2π phase control range, which will allow the arbitrary shaping of light wavefront in full space.

RESULTS AND DISCUSSION

Figure 1a schematically depicts the proposed all-dielectric diatomic metasurface, which is able to convert incident light with arbitrary polarization states into a specific linear polarization. The PMM and PCM are, respectively, designed to be a cylindrical nanodisk and a rectangular nanopillar. It is known that the Jones matrix of such symmetric structure can be expressed as

$$M = \begin{pmatrix} |t_{xx}|e^{i\varphi_{xx}} & 0 \\ 0 & |t_{yy}|e^{i\varphi_{yy}} \end{pmatrix} \tag{1}$$

where $|t_{xx}|$ ($|t_{yy}|$) and φ_{xx} (φ_{yy}) are the transmission amplitude and phase for light polarized along the $x(y)$-axis. By applying a rotation/orientation angle α with respect to the x-axis to the structure, the Jones matrix can be described as

$$M = \begin{pmatrix} \cos\alpha & -\sin\alpha \\ \sin\alpha & \cos\alpha \end{pmatrix} \begin{pmatrix} |t_{xx}|e^{i\varphi_{xx}} & 0 \\ 0 & |t_{yy}|e^{i\varphi_{yy}} \end{pmatrix} \begin{pmatrix} \cos\alpha & \sin\alpha \\ -\sin\alpha & \cos\alpha \end{pmatrix}$$

$$= \begin{pmatrix} |t_{xx}|e^{i\varphi_{xx}}\cos^2\alpha + |t_{yy}|e^{i\varphi_{yy}}\sin^2\alpha & |t_{xx}|e^{i\varphi_{xx}}\cos\alpha\sin\alpha - |t_{yy}|e^{i\varphi_{yy}}\cos\alpha\sin\alpha \\ |t_{xx}|e^{i\varphi_{xx}}\cos\alpha\sin\alpha - |t_{yy}|e^{i\varphi_{yy}}\cos\alpha\sin\alpha & |t_{xx}|e^{i\varphi_{xx}}\sin^2\alpha + |t_{yy}|e^{i\varphi_{yy}}\cos^2\alpha \end{pmatrix} \tag{2}$$

Considering the geometry of the PMM, its Jones matrix is simplified as

$$M_{PMM} = \begin{pmatrix} |t_{xx\_PMM}|e^{i\varphi_{xx\_PMM}} & 0 \\ 0 & |t_{xx\_PMM}|e^{i\varphi_{xx\_PMM}} \end{pmatrix} \tag{3}$$

While for the HWP-like PCM, it is known that there is a phase difference of π between φ_{xx_PCM} and φ_{yy_PCM}. Assuming that $\varphi_{yy\_PCM} - \varphi_{xx\_PCM} = \pi$ and $|t_{xx\_PCM}| = |t_{yy\_PCM}|$, the Jones matrix of the PCM is

$$M_{PCM} = \begin{pmatrix} |t_{xx\_PCM}|e^{i\varphi_{xx\_PCM}}(\cos^2\alpha - \sin^2\alpha) & 2|t_{xx\_PCM}|e^{i\varphi_{xx\_PCM}}\cos\alpha\sin\alpha \\ 2|t_{xx\_PCM}|e^{i\varphi_{xx\_PCM}}\cos\alpha\sin\alpha & |t_{xx\_PCM}|e^{i\varphi_{xx\_PCM}}(\sin^2\alpha - \cos^2\alpha) \end{pmatrix} \tag{4}$$

Furthermore, under the condition that $|t_{xx\_PCM}| = |t_{xx\_PMM}|$ and $\varphi_{xx\_PMM} = \varphi_{xx\_PCM}$, the Jones matrix of the proposed diatomic metasurface can be derived as

$$M_{MS} = M_{PMM} + M_{PCM} = 2|t_{xx\_PMM}|e^{i\varphi_{xx\_PMM}} \begin{pmatrix} \cos^2\alpha & \sin\alpha\cos\alpha \\ \sin\alpha\cos\alpha & \sin^2\alpha \end{pmatrix} \tag{5}$$

Considering a more generalized condition, that is, upon the illumination of an elliptically polarized light represented by $J_{in} = \begin{pmatrix} A_{ox}e^{i\varphi_{ox}} \\ A_{oy}e^{i\varphi_{oy}} \end{pmatrix}$, the transmitted light can be presented as

$$J_{out} = M_{MS}J_{in} = 2|t_{xx\_PMM}|e^{i\varphi_{xx\_PMM}}(A_{ox}e^{i\varphi_{ox}}\cos\alpha + A_{oy}e^{i\varphi_{oy}}\sin\alpha) \begin{pmatrix} \cos\alpha \\ \sin\alpha \end{pmatrix} \tag{6}$$

Equations 5 and 6 indicate that the combination of a proper PMM and PCM can be equivalently considered as a linear polarizer whose polarization angle equals the orientation angle of the PCM, not being affected by the incident polarization state. Furthermore, unlike conventional optical linear polarizers or previously reported monolayer or bilayer plasmonic nanorods, which merely modulate the transmission efficiency, the proposed all-dielectric diatomic metasurface can also tailor the transmitted light phase simultaneously. It should be noted that in our previous work, PMMs and PCMs are also simultaneously incorporated to construct a multifunctional metasurface, where the two meta-atoms are spatially interleaved and considered to operate separately.[38] As a result, triple wavefront shaping functionalities could be achieved by properly setting and viewing designated linear polarization components of both incident and transmitted light. However, for the currently proposed diatomic metasurface, the two meta-atoms are considered as a whole to realize the manipulation of light properties.

With an intention to verify the presented idea, the all-dielectric diatomic metasurface is constructed and evaluated through the finite-difference time-domain (FDTD) method-based tool (FDTD solutions). Similar to our previous work, hydrogenated amorphous silicon (a-Si:H) is used as the material of the meta-atoms which are placed on a glass substrate.[15,38] As depicted in Figure 1a, within a square lattice UC, the a-Si:H PMM and PCM are, respectively, located in the two sub-UCs along the diagonal direction and both designed to be H = 320 nm thick with a center-to-center distance S = 240 nm, which equals the UC periodicity of our previously demonstrated metasurfaces.[15,38] Therefore, the lattice periodicity of the current metasurface design can be derived as $P = \frac{240}{\sqrt{2}} \times 2 = 340$ nm, still less than half of the operation wavelength λ_0 = 690 nm. A PCM operating as a truncated waveguide and guaranteeing highly efficient linear polarization conversion is selected based on our previous work, and the width and length are, respectively, set to be W = 82 nm and L = 154 nm.[15] For the proposed all-dielectric diatomic metasurface, it has been analyzed that the polarization angle of transmitted light is identical to that of the PCM orientation angle, and we first take $\alpha = 45°$ as the example for validation. Here, the PCM orientation angle also represents the angle of the PCM's fast axis with respect to the x-axis. In order to let the beams that are transmitted through the PMM and PCM interfere and give rise to the desired results, we numerically investigated the transmission efficiency and polarization responses of the proposed diatomic metasurface as a function of the PMM nanodisk diameter. For the incident light with polarization parallel to the x-axis, the simulation results shown in Figure 1b–e imply that the PMM diameter has a significant effect on the transmitted light. As indicated by the red circles in Figure 1b,c, the PMM with a diameter of 116 nm is

https://doi.org/10.1021/acsami.1c00967
ACS Appl. Mater. Interfaces 2021, 13, 14497−14506

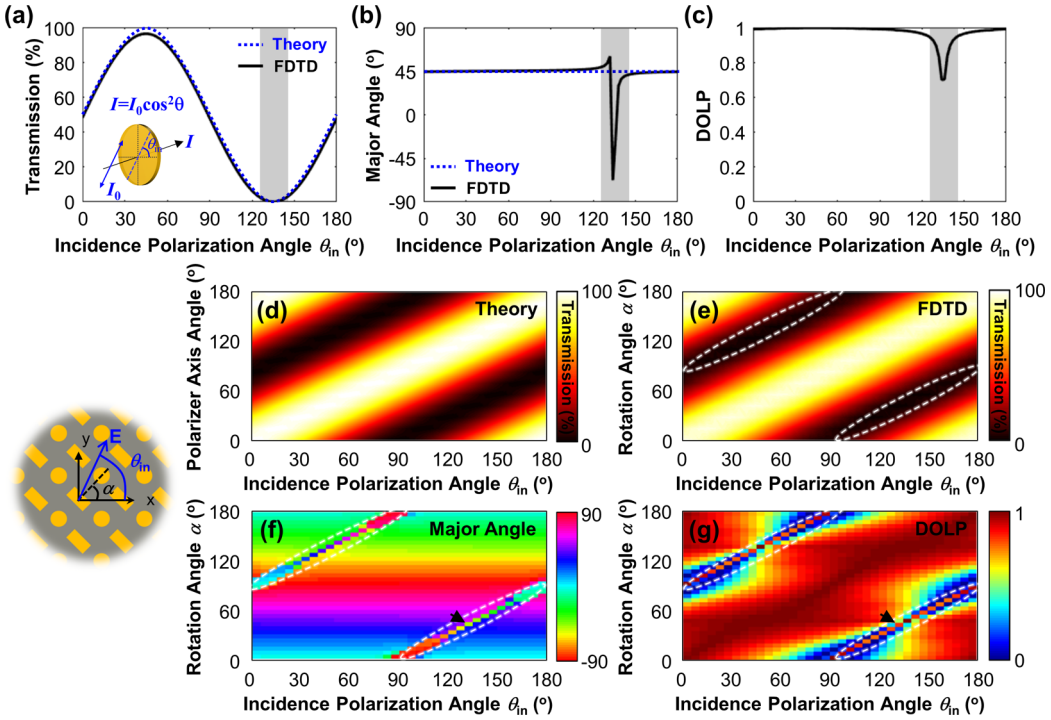

Figure 2. For the designed metasurface, the numerical simulation results of the (a) transmission efficiency, (b) major polarization angle, and (c) DOLP of transmitted light as a function of incidence polarization angle θ_{in}. The blue dotted lines in (a,b) represent the ideal results in theory. (d) For an ideal lossless linear polarizer, the theoretically calculated transmission efficiency with respect to different polarizer axis angle and incidence polarization angle. For the designed metasurface with various PCM rotation angles ranging from 0 to 180°, the simulated (e) transmission, (f) major polarization angle, and (g) DOLP of transmitted light as a function of the incidence polarization angle. The anomaly points indicated by black arrows in (f,g) correspond to the sharp peaks in (b,c).

considered as the optimal candidate. For the constructed diatomic metasurface, the simulated transmission efficiency and major polarization angle are, respectively, found to be 48.1% and 44.3°, which are quite close to the ideal value of 50% and 45° according to the Malus's law and our analysis. The polarization ellipse maps associated with all PMM diameter cases are also depicted in Figure 1d, with the optimal case highlighted in red, showing an excellent linear polarization quality that can be quantitatively evaluated by the degree of linear polarization (DOLP) defined as DOLP = $1 - 2\gamma/(1 + \gamma^2)$, where γ represents the ratio of the lengths of the major to minor axes associated with the ellipse. As can be witnessed in Figure 1e, a high DOLP of 0.99 is accomplished for the optimal case where the diameter of the PMM is 116 nm.

Further numerical simulations are conducted to evaluate the performance of the designed diatomic metasurface. For an ideal lossless linear polarizer with polarization axis along 45°, the theoretical transmission efficiency as a function of incidence polarization angle (θ_{in}) can be predicted according to the Malus's law (blue dotted line in Figure 2a). The corresponding simulation result of the diatomic metasurface is also provided (black solid line), showing good agreements with the theoretical case. The maximum and minimum transmission efficiencies are found to be T_{max} = 96.2% and T_{min} = 0.05% at incidence polarization angles of 45 and 135°, respectively, resulting in a high extinction ratio ER = $10\log(T_{max}/T_{min})$ = 32.8 dB. As investigated and summarized in Figure 2b,c, the major polarization angle and DOLP can also be stably maintained at near 45° and near unity for most incidence polarization angles, despite the deviations within the incidence polarization angle range from 125 to 145° (gray shadowed region), which will be explained later. Considering the low transmission efficiency (less than 2%), we believe the proposed metasurface linear polarizer still can be used in application fields such as binary-image display or information encoding.[30] In addition, it has also been reported that for an incident light with a fixed polarization state, a continuous light intensity modulation can be realized by rotating the nanoscale linear polarizer.[26] Yet, this strategy may not be suitably applied in our proposed metasurface since two different meta-atoms are incorporated in one UC. However, it is worth noting that our theoretical analysis predicts that the polarization axis of the metasurface linear polarizer equals the rotation angle of the PCM, providing a simplified and reliable approach than the previous works where both meta-atoms are inevitably required to be rotated.[35] Subsequently, multiple simulations are carried out to check the effect of the PCM orientation angle on the metasurface performance. First, for an ideal lossless linear polarizer, the transmission efficiency as a function of the incidence polarization angle for various polarizer axis angles can be theoretically estimated, as plotted in Figure 2d. The transmission peak (dip) occurs when the incidence polarization is parallel (perpendicular) to the polarizer axis. For the designed diatomic metasurface, the transmission distributions for various PCM orientation angles are simulated, as illustrated in Figure 2e, which is in high consistency with the theoretical result. Presented in Figure 2f,g are the simulation results of the major polarization angle and DOLP of transmitted light. It is clear that upon the illumination of linearly polarized light, the major polarization angle for most incidence polarization angles remains nearly invariant at a value equaling to the PCM orientation angle as expected. It is worth noting that some

https://doi.org/10.1021/acsami.1c00967
ACS Appl. Mater. Interfaces 2021, 13, 14497−14506

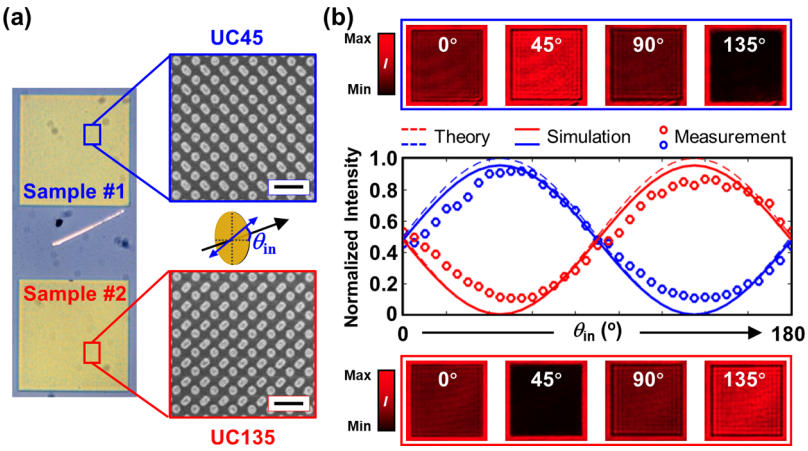

Figure 3. (a) Microscopy and SEM images of the two fabricated metasurface samples. The scale bars both represent 500 nm. (b) Experimentally observed transmitted light intensity profiles at incidence polarization angles of 0, 45, 90, and 135°. Measured transmission efficiencies of the two samples under various incidence polarization angles.

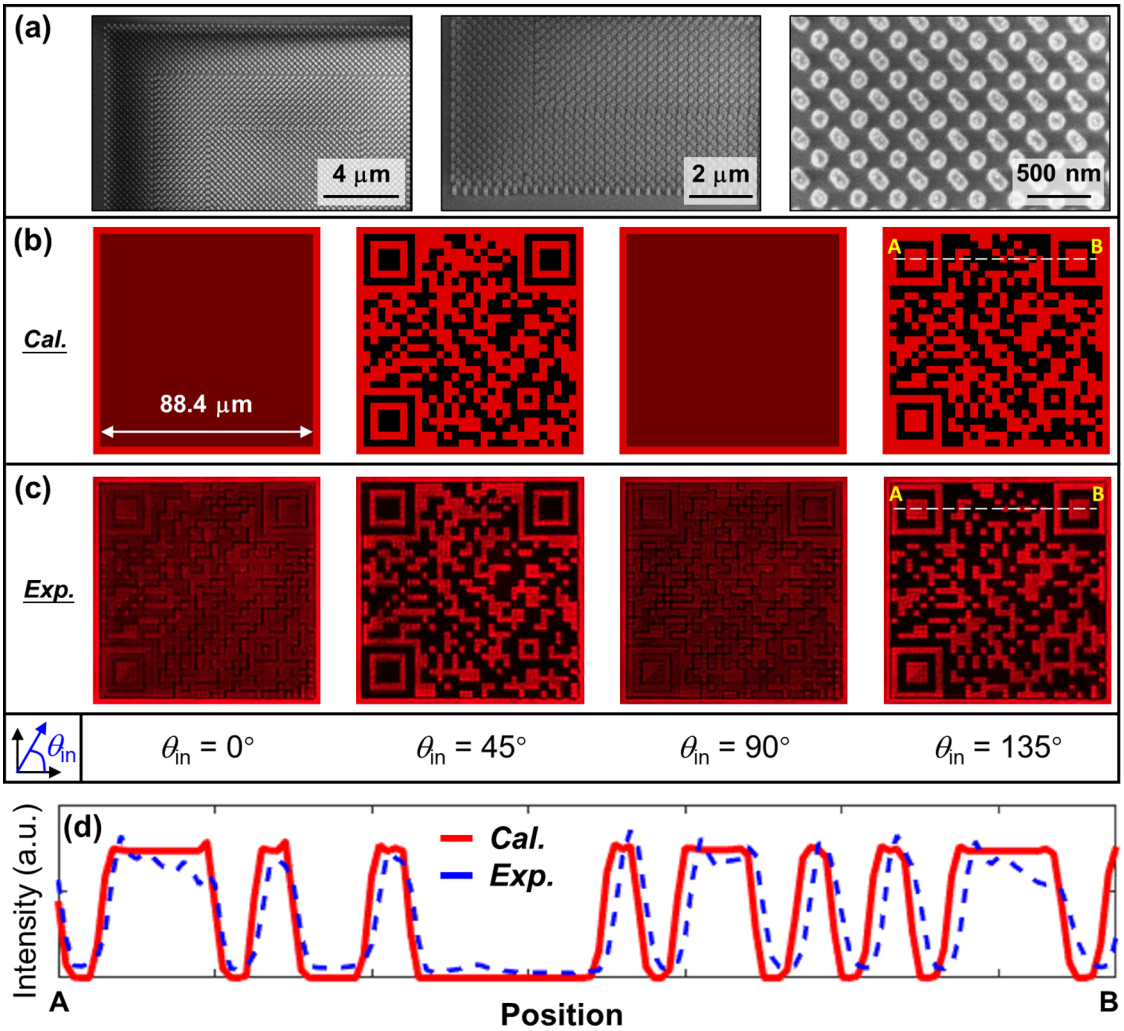

Figure 4. (a) SEM images of the fabricated metasurface QR code. The QR code pattern in (b) theoretical calculation and (c) measurement at incidence polarization angles of 0, 45, 90, and 135°. (d) Extracted intensity value along the dashed line from A to B marked in (b,c).

anomaly points can be seen in the white dashed line region which could be qualitatively explained below. As can be understood, for the incident light with polarization angle of θ, the transmitted light from the PMM holds the same polarization angle, whereas the PCM will alter the polarization angle into $2\alpha-\theta$ when its fast axis is set along α, and they will keep identical polarization angle difference with respect to the PCM orientation angle. As long as the two light beams can be decomposed and have a field component along α, it is possible to attain this fixed polarization component in the transmission

https://doi.org/10.1021/acsami.1c00967
ACS Appl. Mater. Interfaces 2021, 13, 14497−14506

space. Nevertheless, for the white dashed line region where the incidence polarization is approaching to the situation when it is orthogonal to the fast axis of the PCM, that is, $\theta = \alpha \pm 90°$, the polarization angles of the light transmitted from the PMM and PCM both equal $\alpha \pm 90°$ and thus no field component can be derived along α. It can be anticipated that as the incidence polarization angle is approaching the critical condition ($\theta = \alpha \pm 90°$), small variations of the amplitude and phase of the transmitted light fields are likely to give rise to an elliptical polarization instead of a rigorous linear one. Note that the sharp peaks that appeared in Figure 2b,c correspond to the anomaly points in Figure 2f,g (black arrows). While the polarization angle and DOLP within the white dashed region deviate a lot, the corresponding transmission efficiencies maintain at a low level. Besides, the deteriorated polarization quality could be addressed by taking advantage of the multilayer design strategy. For example, by vertically stacking multiple layers of the designed metasurfaces, the DOLP can be greatly improved with an average value of 0.986, while the number of deviations of the major angle and DOLP can also be largely reduced (Figure S1 in the Supporting Information).

In order to experimentally validate our claims, two metasurface linear polarizer samples (sample #1 and #2), of which the PCMs are, respectively, rotated by 45 and 135° (the corresponding UCs are referred to as UC45 and UC135 hereafter), are manufactured through standard electron beam lithography, lift-off, and etching techniques, similar to our previous work.[39] Each sample consists of 88 × 88 UCs that corresponds to a dimension of approximately 30 μm × 30 μm, and details of the fabrication procedure are available in the Materials and Methods section. The optical microscopy and scanning electron microscopy (SEM) images of the fabricated samples (labeled as UC45 and UC135) are shown in Figure 3a. The samples are subsequently characterized with the help of a custom-built measurement setup (Figure S2 in the Supporting Information), where a narrowband filter ("FB690-10", Thorlabs) paired with a linear polarizing film ("XP42-75", Edmund Optics) that is fixed on a Glan-Thompson polarizer holder are placed between a supercontinuum laser ("SuperK compact", NKT Photonics) and the sample. A customized imaging system containing a 50×/0.4 objective, tube lens, and CCD camera is placed behind the sample to record the profile of transmitted light intensity. For each sample, a series of light intensity profiles are captured by varying the incidence polarization angle from 0 to 180° in a step of 5°, and Figure 3b displays the relevant results at polarization angles of 0, 45, 90, and 135°. The light intensity change as a function of the polarization angle is further estimated by integrating the intensity value within the metasurface area. Taking a substrate region with an identical area but no metasurface pattern as the reference, the results are further normalized, as indicated by the blue and red circles in Figure 3b, where an overall good match between the measurement and simulation results can be found. The nonzero minimum intensity value could be attributed to the roundness/roughness of the surface, corners, and edge of the nanopillars and nanodisks, as is validated through additional simulation results illustrated in Supporting Information Figure S3. It can be inferred from these measurement results that the polarization angles of the two metasurface linear polarizers are in the vicinity of 45 and 135°, respectively.

In light of its salient performance in attaining high-intensity contrast, UC45 and UC135 are simultaneously utilized to encrypt a QR code linking to the logo of "University of Jinan". The metasurface QR code is composed of 260 × 260 UCs, which translates to a metasurface area of 88.4 μm × 88.4 μm, with a minimum pixel width of 2.72 μm. The SEM images of the fabricated metasurface QR code, along with the theoretically calculated and experimentally measured transmission light intensity profiles, are provided in Figure 4a–c. It is apparent that there is a maximum intensity contrast between UC45 and UC135 at the incidence polarization angles of 45 and 135°, which leads to the appearance of the original and the complement QR code, whereas at incidence polarization angles of 0 and 90°, no QR code pattern can be obtained due to the similar transmission intensities. The intensity data along the dashed line from A to B as marked in Figure 4b,c are extracted and plotted in Figure 4d for better comparison. In Figure 4c, note that at incidence polarization angles of 0 and 90°, unlike the intensity distribution which is smooth and uniform in theory, the contour of the QR code can be roughly seen from the measured results. This can be attributed to the imperfect alignment of the two types of UCs (UC45 and UC135) during fabricating the metasurface QR code, as can be indicated from the SEM images in Figure 4a. Overall, there is a good match between the calculation and measurement results in terms of the intensity variation trend. For the fabricated samples, the evolutions of their transmitted light intensity profiles with varying incidence polarization angles can be seen in Videos S1 and S2 in the Supporting Information. The stored information can be decrypted by scanning the intensity patterns using the camera of a smartphone. An example illustrating the decryption process can be found in Video S3 in the Supporting Information. According to the simulation results of Figure 2, we further anticipate that PCMs with various orientation angles can be simultaneously utilized for yielding multiple grayscale intensity levels and therefore can be applied in applications such as grayscale image display and information encryption.

While the previously reported nanoscale linear polarizer based on a single type of meta-atom (such as a silver nanorod) has shown its powerful capability in light intensity control, its ability in modulating the same polarized light phase is severely limited.[32] For example, even if taking no account of the transmission efficiency, the nanorod with a wide range of different lateral dimensions can only provide a phase modulation range (difference between maximum and minimum phase) of $\sim 0.8\pi$ (Figure S4 in the Supporting Information). Here, we demonstrate that the proposed diatomic metasurface can easily yield a notable phase difference of π while maintaining high transmission efficiencies. For the previously designed PCM with an orientation angle α, if the orientation angle is changed to $\alpha' = \alpha + 90°$, its Jones matrix can be rewritten as

$$M'_{\mathrm{PCM}} = \begin{pmatrix} |t_{xx\_\mathrm{PCM}}|e^{i\varphi_{xx\_\mathrm{PCM}}}(\sin^2\alpha - \cos^2\alpha) & -2|t_{xx\_\mathrm{PCM}}|e^{i\varphi_{xx\_\mathrm{PCM}}}\cos\alpha\sin\alpha \\ -2|t_{xx\_\mathrm{PCM}}|e^{i\varphi_{xx\_\mathrm{PCM}}}\cos\alpha\sin\alpha & |t_{xx\_\mathrm{PCM}}|e^{i\varphi_{xx\_\mathrm{PCM}}}(\cos^2\alpha - \sin^2\alpha) \end{pmatrix} \quad (7)$$

Based on eq 7 and our previous analysis, it is known that if the new PCM is paired with the previously designed PMM (|

https://doi.org/10.1021/acsami.1c00967
ACS Appl. Mater. Interfaces 2021, 13, 14497−14506

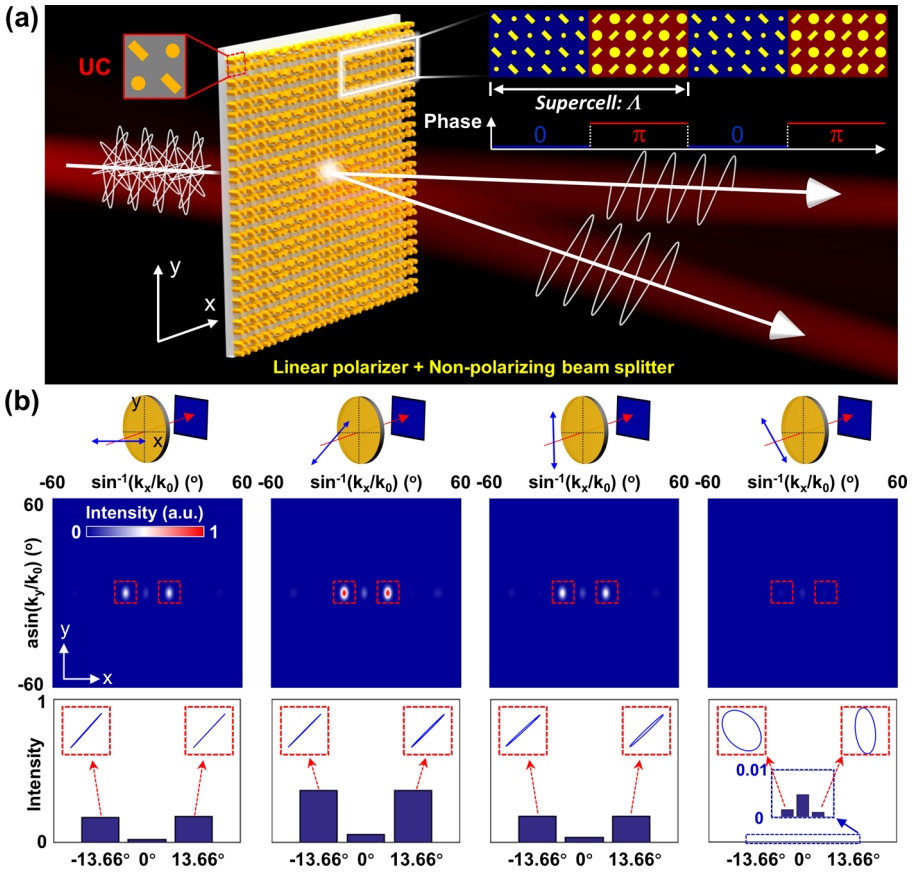

Figure 5. (a) Schematic of the proposed metasurface beam splitter which is equivalent to the integration of a linear polarizer (with polarization axis along 45°) and a nonpolarizing beam splitter. (b) Simulated far-field intensity profiles and normalized transmission intensities at incidence polarization angles of 0, 45, 90, and 135°. The polarization ellipse relating to each split beam is also depicted.

$t_{xx\_PMM}| = |t_{xx\_PCM}|$ and $\varphi_{xx\_PMM} = \varphi_{xx\_PCM}$), then the metasurface linear polarizer will simply change its polarization axis to $\alpha + 90°$. However, if one considers a new PMM that satisfy $|t'_{xx\_PMM}| = |t_{xx\_PCM}| = |t_{xx\_PMM}|$ and $\varphi'_{xx\_PMM} = \varphi_{xx\_PCM} + \pi$ (i.e., $\varphi'_{xx\_PMM} = \varphi_{yy\_PCM}$), where t'_{xx_PMM} and φ'_{xx_PMM}, respectively, represent the transmission amplitude and phase of the new PMM, after a few derivation processes, the Jones matrix of the new diatomic metasurface will be modified to

$$M'_{MS} = M'_{PMM} + M'_{PCM} = 2|t_{xx\_PMM}|e^{i\varphi'_{xx\_PMM}}\begin{pmatrix}\cos^2\alpha & \sin\alpha\cos\alpha\\ \sin\alpha\cos\alpha & \sin^2\alpha\end{pmatrix} \quad (8)$$

Equations 5 and 8 imply that two metasurface linear polarizers can be designed to have the identical polarization angle and meanwhile impart a π phase difference to the transmitted light; in other words, we could easily obtain a 1-bit phase control (state "0" and "1" correspond to phase "0" and "π", respectively) based on the proposed dielectric diatomic metasurface, which outperforms other dielectric diatomic metasurface that mainly manipulates the polarization.[35] Compared to its plasmonic counterpart, such an all-dielectric diatomic metasurface enabling the 1-bit phase modulation feature could be considered as an efficient digital coding metasurface for manipulating visible light.[40]

The 1-bit phase tuning ability of the proposed diatomic metasurface is subsequently highlighted through demonstration of a novel application. As schematically illustrated in Figure 5a, by alternatively arranging the two metasurface UCs, a metasurface beam splitter that can be functionally treated as the integration of a linear polarizer and a nonpolarizing beam splitter can be expectedly attained. For a fixed PCM, with an increase of the PMM diameter, mutual near-field couplings between the PMM and PCM could occur, which may in turn disturb the transmission and polarization responses of the PCM and PMM. To avoid this, we design a new UC with a relatively large lattice periodicity (P = 480 nm, $\sim 0.7\lambda_0$) and arrange a pair of PMMs and PCMs in it as can be witnessed in the top-left inset in Figure 5a. It should be noted that the metasurface should be designed with a proper lattice periodicity so that the designed polarization states with high transmission efficiency can be attained. Neither should it be designed too small as mutual near-field couplings will emerge,[41,42] which will distort the original polarization and phase responses of the meta-atom, nor should it be too large as the maximum and minimum transmission could be, respectively, decreased and increased when the meta-atoms are too sparsely located. More details on the effect of the lattice periodicity on the metasurface performance can be found in Figure S5 in the Supporting Information. Similarly, the metasurface linear polarizer with the polarization angle at 45° is taken as an example to prove our claim. For the UC which imparts a relative phase delay of 0, the PCM and PMM dimensions are same as that of the design relevant to Figure 2, and the PCM is rotated by 45°. For the UC that imparts a relative phase delay of π, the PCM orientation angle is changed from 45 to 135°, while the PMM diameter is optimized to be

https://doi.org/10.1021/acsami.1c00967
ACS Appl. Mater. Interfaces 2021, 13, 14497−14506

179 nm. The relevant simulation results and details for determining the PMM diameter can be found in Figure S6 in the Supporting Information. Under normally incident light, the beam splitting angle (half angle) can be theoretically predicted following the generalized Snell's law: $\theta_{out} = \sin^{-1}(\lambda_0/\Lambda)$, where Λ is the length of the beam splitter supercell. Here, the supercell constitutes six UCs (Λ = 2.88 μm) along the x-axis and thus the splitting angle can be derived as θ_{out} = 13.86°. The simulated far-field profiles of the transmission intensity at incidence polarization angles of 0, 45, 90, and 135° are provided in Figure 5b. Particularly for the former three cases, the normally incident light is mainly directed to two opposite directions with nearly equal optical power at oblique angles of −13.66 and 13.66°, which are quite close to the theoretically calculated splitting angle. The total transmission efficiency of the two split beams reaches a maximum and minimum value of ∼73 and ∼0.25% at incidence polarization angles of 45 and 135°, respectively. The simulated polarization ellipses of the two split beams further reveal that the designed metasurface is equivalent to the integration of a linear polarizer (with polarization axis along 45°) and a nonpolarizing beam splitter. Note that while the polarization purities of the split beams are high, the intensities of split beams are less efficient since in addition to the desired diffraction order, the transmitted light can be found at numerous other diffraction orders. Details of the simulated transmission in each diffraction order are provided in Figure S7 in the Supporting Information. Moreover, by simultaneously rotating all PCMs with identical angle, the polarization angle of the split beams can be accordingly adjusted, which is unattainable with conventional optical components or previously demonstrated metasurface beam splitters. The simulation results for several beam splitter designs with polarization angles of 135, 0, and 30° can be found in Figure S8 in the Supporting Information. A comparison between the proposed beam splitter and conventional or other metasurface-based polarizing/nonpolarizing beam splitters is also available in Figure S9 in the Supporting Information. Note that the metasurface beam splitter can be fabricated following the same procedures as described in the Materials and Methods section. Additionally, the effects of the angle of incidence and wavelength on the proposed metasurface beam splitter are further investigated numerically, as can be seen in Figures S10 and S11 in the Supporting Information. It is apparent that the proposed metasurface beam splitter exhibits an extremely thin volume, which can be greatly beneficial in the miniaturization of the relevant photonic system. We anticipate that the phase tuning range of the designed diatomic metasurface can be potentially extended to cover the entire 2π range; therefore, more versatile wavefront manipulation functionalities can be achieved.

CONCLUSIONS

In conclusion, we proposed a single-layer all-dielectric diatomic metasurface consisting of a-Si:H-based PMM and PCM. By virtue of rigorous theoretical analyses and numerical simulations, we systematically investigated its transmission and polarization responses as a function of the PMM diameter and incidence polarization angles. The results showed that the optimized diatomic metasurface can functionally operate as a nanoscale linear polarizer whose polarization angle is correlated to the orientation angle of the PCM, and the diatomic metasurface exhibited excellent performances including a maximum transmission efficiency of 96.2% and an ER of 32.8 dB. Two metasurface samples designed with orthogonal linear polarization angles of 45 and 135° were fabricated and experimentally characterized. Based on their superior intensity contrast, a metasurface QR code pattern was further manufactured by simultaneously incorporating the two metasurface UCs to demonstrate its potential application in a binary-image display or information encoding. In addition, unlike conventional linear polarizers that merely modulate the light intensity, we showed that the proposed metasurface can also implement a π phase modulation. As such, a set of metasurface beam splitters that are equivalent to the integration of a nonpolarizing beam splitter and linear polarizer (with different polarization angles) were numerically demonstrated. By further expanding its phase tuning range, we expect that a variety of metadevices enabling various wavefront shaping functionalities could be accomplished in the future.

MATERIALS AND METHODS

The proposed metasurfaces were produced on a microscopic slide glass. First, the substrate was cleaned using acetone/isopropyl alcohol/deionized water in order to promote its adhesion to the hydrogenated amorphous silicon (a-Si:H) film. Plasma-enhanced chemical vapor deposition (PlasmaLab 100 from Oxford) was applied to deposit 320 nm thick a-Si:H films on the glass using SiH_4 and helium as precursor gases. Then, a positive electron beam resist, ZEP520A, was spin-coated on the substrate. Subsequently, E-spacers 300Z from Showa Denko was coated to prevent charging during electron beam exposure. The metasurfaces were written on the resist using electron-beam lithography (Raith150), accompanied by development in the ZED-N50 solvent. A 40 nm thick Al film was deposited via electron beam evaporation (Temescal BJD-2000) on the surface, and it was patterned by lifting off the resist in a solvent (ZDMAC from Zeon Co.). The patterned Al was utilized as a hard mask during dry etching, thereby transferring the designed pattern to the underlying a-Si:H layer through fluorine-based inductively coupled plasma-reactive ion etching (Oxford PlasmaLab System 100). Next, the wet etching was carried out to remove the residual Al from the patterned nanopillars.

ASSOCIATED CONTENT

Supporting Information

The Supporting Information is available free of charge at https://pubs.acs.org/doi/10.1021/acsami.1c00967.

Simulated transmission and polarization responses for four-layered diatomic metasurfaces, effect of structure morphology changes on the performance of the metasurface polarizer, simulated transmission and phase responses of a silver nanorod placed on a glass substrate, schematic of the measurement setup, effect of period size on the performance of the new metasurface UC, simulation results of the newly designed metasurface linear polarizer imparting phase delay of "0" and "π", simulated efficiency in various diffraction orders, simulation results of metasurface beam splitters exhibiting various polarization angles, comparison of several types of beam splitters, effect of angle of incidence on the diatomic metasurface, and broadband response of the diatomic metasurface (PDF)

Transmission light intensity profiles for samples #1 and #2 illuminated with varying incidence polarization angles (MP4)

Transmission light intensity profiles for the metasurface QR code sample illuminated with varying incidence polarization angles (MP4)

https://doi.org/10.1021/acsami.1c00967
ACS Appl. Mater. Interfaces 2021, 13, 14497−14506

Decryption process of the information stored in the QR code by scanning it through the camera of a smartphone (MP4)

AUTHOR INFORMATION

Corresponding Authors

Wenjing Yue − *School of Information Science and Engineering and Shandong Provincial Key Laboratory of Network Based Intelligent Computing, University of Jinan, Jinan, Shandong 250022, China*; Email: ise_yuewj@ujn.edu.cn

Yang Li − *School of Information Science and Engineering and Shandong Provincial Key Laboratory of Network Based Intelligent Computing, University of Jinan, Jinan, Shandong 250022, China*; orcid.org/0000-0001-5260-5157; Email: ise_liy@ujn.edu.cn

Authors

Song Gao − *School of Information Science and Engineering and Shandong Provincial Key Laboratory of Network Based Intelligent Computing, University of Jinan, Jinan, Shandong 250022, China*

Changyi Zhou − *Department of Electronic Engineering and Nano Device Application Center, Kwangwoon University, Seoul 01897, South Korea*

Chunwei Zhang − *School of Information Science and Engineering and Shandong Provincial Key Laboratory of Network Based Intelligent Computing, University of Jinan, Jinan, Shandong 250022, China*

Hao Kan − *School of Information Science and Engineering and Shandong Provincial Key Laboratory of Network Based Intelligent Computing, University of Jinan, Jinan, Shandong 250022, China*

Chao Li − *School of Information Science and Engineering and Shandong Provincial Key Laboratory of Network Based Intelligent Computing, University of Jinan, Jinan, Shandong 250022, China*

Sang-Shin Lee − *Department of Electronic Engineering and Nano Device Application Center, Kwangwoon University, Seoul 01897, South Korea*

Duk-Yong Choi − *Laser Physics Centre, Research School of Physics, Australian National University, Canberra, Australian Capital Territory 2601, Australia*; orcid.org/0000-0002-5339-3085

Complete contact information is available at: https://pubs.acs.org/10.1021/acsami.1c00967

Notes

The authors declare no competing financial interest.

ACKNOWLEDGMENTS

This work was supported by the National Natural Science Foundation of China under grant (61805101, 62005095, 61604060, and 61905091), the Shandong Provincial Natural Science Foundation under grant (ZR2020QF105, ZR2017JL027, ZR2018BF025, and ZR2019BF013), and the Shandong Province Key Research and Development Program (2019RKB01023). This research was supported by the Basic Science Research Program through the National Research Foundation of Korea (NRF), funded by the Ministry of Education (no. 2018R1A6A1A03025242) and the Ministry of Science and ICT (2020R1A2C3007007), and was performed in part at the ACT node of the Australian National Fabrication Facility. The present research has been conducted by the Excellent researcher support project of Kwangwoon University in 2021.

ABBREVIATIONS

HWP, half-wave plate
PCM, polarization-converting meta-atom
UC, unit cell
PMM, polarization-maintaining meta-atom
QR, quick response
FDTD, finite-difference time-domain
DOLP, degree of linear polarization
SEM, scanning electron microscopy

REFERENCES

(1) Yu, N.; Genevet, P.; Kats, M. A.; Aieta, F.; Tetienne, J.-P.; Capasso, F.; Gaburro, Z. Light Propagation with Phase Discontinuities: Generalized Laws of Reflection and Refraction. *Science* **2011**, *334*, 333−337.

(2) Khorasaninejad, M.; Chen, W. T.; Devlin, R. C.; Oh, J.; Zhu, A. Y.; Capasso, F. Metalenses at Visible Wavelengths: Diffraction-Limited Focusing and Subwavelength Resolution Imaging. *Science* **2016**, *352*, 1190−1194.

(3) Wang, B.; Dong, F.; Li, Q.-T.; Yang, D.; Sun, C.; Chen, J.; Song, Z.; Xu, L.; Chu, W.; Xiao, Y.-F.; Gong, Q.; Li, Y. Visible-Frequency Dielectric Metasurfaces for Multiwavelength Achromatic and Highly Dispersive Holograms. *Nano Lett.* **2016**, *16*, 5235−5240.

(4) Mehmood, M. Q.; Mei, S.; Hussain, S.; Huang, K.; Siew, S. Y.; Zhang, L.; Zhang, T.; Ling, X.; Liu, H.; Teng, J.; Danner, A.; Zhang, S.; Qiu, C.-W. Visible-Frequency Metasurface for Structuring and Spatially Multiplexing Optical Vortices. *Adv. Mater.* **2016**, *28*, 2533−2539.

(5) Chen, S.; Li, Z.; Liu, W.; Cheng, H.; Tian, J. From Single-Dimensional to Multidimensional Manipulation of Optical Waves with Metasurfaces. *Adv. Mater.* **2019**, *31*, 1802458.

(6) Chen, S.; Liu, W.; Li, Z.; Cheng, H.; Tian, J. Metasurface-Empowered Optical Multiplexing and Multifunction. *Adv. Mater.* **2020**, *32*, 2070022.

(7) Wu, Z.; Powers, P. E.; Sarangan, A. M.; Zhan, Q. Optical Characterization of Wiregrid Micropolarizers Designed for Infrared Imaging Polarimetry. *Opt. Lett.* **2008**, *33*, 1653−1655.

(8) Shin, Y. J.; Wu, Y.-K.; Lee, K.-T.; Ok, J. G.; Guo, L. J. Fabrication and Encapsulation of a Short-Period Wire Grid Polarizer with Improved Viewing Angle by the Angled-Evaporation Method. *Adv. Opt. Mater.* **2013**, *1*, 863−868.

(9) Kruk, S.; Hopkins, B.; Kravchenko, I. I.; Miroshnichenko, A.; Neshev, D. N.; Kivshar, Y. S. Invited Article: Broadband Highly Efficient Dielectric Metadevices for Polarization Control. *APL Photonics* **2016**, *1*, 030801.

(10) Khorasaninejad, M.; Zhu, W.; Crozier, K. B. Efficient Polarization Beam Splitter Pixels Based on a Dielectric Metasurface. *Optica* **2015**, *2*, 376−382.

(11) Jiang, Z. H.; Lin, L.; Ma, D.; Yun, S.; Werner, D. H.; Liu, Z.; Mayer, T. S. Broadband and Wide Field-of-View Plasmonic Metasurface-Enabled Waveplates. *Sci. Rep.* **2015**, *4*, 7511.

(12) Yang, Y.; Wang, W.; Moitra, P.; Kravchenko, I. I.; Briggs, D. P.; Valentine, J. Dielectric Meta-Reflectarray for Broadband Linear Polarization Conversion and Optical Vortex Generation. *Nano Lett.* **2014**, *14*, 1394−1399.

(13) Ding, F.; Wang, Z.; He, S.; Shalaev, V. M.; Kildishev, A. V. Broadband High-Efficiency Half-Wave Plate: A Supercell-Based Plasmonic Metasurface Approach. *ACS Nano* **2015**, *9*, 4111−4119.

(14) Arbabi, A.; Horie, Y.; Bagheri, M.; Faraon, A. Dielectric Metasurfaces for Complete Control of Phase and Polarization with Subwavelength Spatial Resolution and High Transmission. *Nat. Nanotechnol.* **2015**, *10*, 937−943.

(15) Gao, S.; Park, C.-S.; Lee, S.-S.; Choi, D.-Y. All-Dielectric Metasurfaces for Simultaneously Realizing Polarization Rotation and Wavefront Shaping of Visible Light. *Nanoscale* **2019**, *11*, 4083−4090.
(16) Ding, F.; Chen, Y.; Bozhevolnyi, S. I. Gap-Surface Plasmon Metasurfaces for Linear-Polarization Conversion, Focusing, and Beam Splitting. *Photon. Res.* **2020**, *8*, 707−714.
(17) Ding, F.; Deshpande, R.; Meng, C.; Bozhevolnyi, S. I. Metasurface-Enabled Broadband Beam Splitters Integrated with Quarter-Wave Plate Functionality. *Nanoscale* **2020**, *12*, 14106−14111.
(18) Hu, Y.; Wang, X.; Luo, X.; Ou, X.; Li, L.; Chen, Y.; Ping Yang, P.; Wang, S.; Duan, H. All-Dielectric Metasurfaces for Polarization Manipulation: Principles and Emerging Applications. *Nanophotonics* **2020**, *9*, 3755−3780.
(19) Wu, P. C.; Tsai, W.-Y.; Chen, W. T.; Huang, Y.-W.; Chen, T.-Y.; Chen, J.-W.; Liao, C. Y.; Chu, C. H.; Sun, G.; Tsai, D. P. Versatile Polarization Generation with an Aluminum Plasmonic Metasurface. *Nano Lett.* **2016**, *17*, 445−452.
(20) Huang, Y.; Xie, X.; Pu, M.; Guo, Y.; Xu, M.; Ma, X.; Li, X.; Luo, X. Dual-Functional Metasurface Toward Giant Linear and Circular Dichroism. *Adv. Opt. Mater.* **2020**, *8*, 1902061.
(21) Zi, J.; Li, Y.; Feng, X.; Xu, Q.; Liu, H.; Zhang, X.-X.; Han, J.; Zhang, W. Dual-Functional Terahertz Waveplate Based on All-Dielectric Metamaterial. *Phys. Rev. Appl.* **2020**, *13*, 034042.
(22) Yue, F.; Zhang, C.; Zang, X.-F.; Wen, D.; Gerardot, B. D.; Zhang, S.; Chen, X. High-Resolution Grayscale Image Hidden in a Laser Beam. *Light Sci. Appl.* **2018**, *7*, 17129.
(23) Zang, X.; Dong, F.; Yue, F.; Zhang, C.; Xu, L.; Song, Z.; Chen, M.; Chen, P.-Y.; Buller, G. S.; Zhu, Y.; Zhuang, S.; Chu, W.; Zhang, S.; Chen, X. Polarization Encoded Color Image Embedded in a Dielectric Metasurface. *Adv. Mater.* **2018**, *30*, 1707499.
(24) Zhao, R.; Huang, L.; Tang, C.; Li, J.; Li, X.; Wang, Y.; Zentgraf, T. Nanoscale Polarization Manipulation and Encryption Based on Dielectric Metasurfaces. *Adv. Opt. Mater.* **2018**, *6*, 1800490.
(25) Zhang, C.; Wen, D.; Yue, F.; Intaravanne, Y.; Wang, W.; Chen, X. Optical Metasurface Generated Vector Beam for Anticounterfeiting. *Phys. Rev. Appl.* **2018**, *10*, 034028.
(26) Wang, L.; Li, T.; Guo, R. Y.; Xia, W.; Xu, X. G.; Zhu, S. N. Active Display and Encoding by Integrated Plasmonic Polarizer on Light-Emitting-Diode. *Sci. Rep.* **2013**, *3*, 2603.
(27) Dai, Q.; Deng, L.; Deng, J.; Tao, J.; Yang, Y.; Chen, M.; Li, Z.; Li, Z.; Zheng, G. Ultracompact, High-Resolution and Continuous Grayscale Image Display Based on Resonant Dielectric Metasurfaces. *Opt. Express* **2019**, *27*, 27927−27935.
(28) Zhang, Y.; Cheng, Y.; Chen, M.; Xu, R.; Yuan, L. Ultracompact Metaimage Display and Encryption with a Silver Nanopolarizer Based Metasurface. *Appl. Phys. Lett.* **2020**, *117*, 021105.
(29) Deng, J.; Deng, L.; Guan, Z.; Tao, J.; Li, G.; Li, Z.; Li, Z.; Yu, S.; Zheng, G. Multiplexed Anticounterfeiting Meta-Image Displays with Single-Sized Nanostructures. *Nano Lett.* **2020**, *20*, 1830−1838.
(30) Dai, Q.; Zhou, N.; Deng, L.; Deng, J.; Li, Z.; Zheng, G. Dual-Channel Binary Gray-Image Display Enabled with Malus-Assisted Metasurfaces. *Phys. Rev. Appl.* **2020**, *14*, 034002.
(31) Li, Z.; Liu, W.; Cheng, H.; Choi, D. Y.; Chen, S.; Tian, J. Arbitrary Manipulation of Light Intensity by Bilayer Aluminum Metasurfaces. *Adv. Opt. Mater.* **2019**, *7*, 1900260.
(32) Deng, L.; Deng, J.; Guan, Z.; Tao, J.; Chen, Y.; Yang, Y.; Zhang, D.; Tang, J.; Li, Z.; Li, Z.; Yu, S.; Zheng, G.; Xu, H.; Qiu, C.-W.; Zhang, S. Malus-Metasurface-Assisted Polarization Multiplexing. *Light Sci. Appl.* **2020**, *9*, 101.
(33) Deng, Z.-L.; Deng, J.; Zhuang, X.; Wang, S.; Li, K.; Wang, Y.; Chi, Y.; Ye, X.; Xu, J.; Wang, G. P.; Zhao, R.; Wang, X.; Cao, Y.; Cheng, X.; Li, G.; Li, X. Diatomic Metasurface for Vectorial Holography. *Nano Lett.* **2018**, *18*, 2885−2892.
(34) Deng, Z. L.; Jin, M.; Ye, X.; Wang, S.; Shi, T.; Deng, J.; Mao, N.; Cao, Y.; Guan, B. O.; Alù, A.; Li, G.; Li, X. Full-Color Complex-Amplitude Vectorial Holograms Based on Multi-Freedom Metasurfaces. *Adv. Funct. Mater.* **2020**, *30*, 1910610.
(35) Wang, S.; Deng, Z.-L.; Wang, Y.; Zhou, Q.; Wang, X.; Cao, Y.; Guan, B.-O.; Xiao, S.; Li, X. Arbitrary Polarization Conversion Dichroism Metasurfaces for All-in-One Full Poincaré Sphere Polarizers. *Light Sci. Appl.* **2021**, *10*, 24.
(36) Yang, Q.; Chen, X.; Xu, Q.; Tian, C.; Xu, Y.; Cong, L.; Zhang, X.; Li, Y.; Zhang, C.; Zhang, X.; Han, J.; Zhang, W. Broadband Terahertz Rotator with an All-Dielectric Metasurface. *Photon. Res.* **2018**, *6*, 1056−1061.
(37) Sisler, J.; Chen, W. T.; Zhu, A. Y.; Capasso, F. Controlling Dispersion in Multifunctional Metasurfaces. *APL Photonics* **2020**, *5*, 056107.
(38) Gao, S.; Park, C. S.; Zhou, C.; Lee, S. S.; Choi, D. Y. Twofold Polarization-Selective All-Dielectric Trifoci Metalens for Linearly Polarized Visible Light. *Adv. Opt. Mater.* **2019**, *7*, 1900883.
(39) Gao, S.; Park, C. S.; Lee, S. S.; Choi, D. Y. A Highly Efficient Bifunctional Dielectric Metasurface Enabling Polarization-Tuned Focusing and Deflection for Visible Light. *Adv. Opt. Mater.* **2019**, *7*, 1801337.
(40) Cui, T. J.; Qi, M. Q.; Wan, X.; Zhao, J.; Cheng, Q. Coding Metamaterials, Digital Metamaterials and Programmable Metamaterials. *Light Sci. Appl.* **2014**, *3*, No. e218.
(41) Deshpande, R.; Zenin, V. A.; Ding, F.; Mortensen, N. A.; Bozhevolnyi, S. I. Direct Characterization of Near-Field Coupling in Gap Plasmon-Based Metasurfaces. *Nano Lett.* **2018**, *18*, 6265−6270.
(42) Lepeshov, S.; Kivshar, Y. Near-Field Coupling Effects in Mie-Resonant Photonic Structures and All-Dielectric Metasurfaces. *ACS Photonics* **2018**, *5*, 2888−2894.

https://doi.org/10.1021/acsami.1c00967
ACS Appl. Mater. Interfaces 2021, 13, 14497−14506